



HAL
open science

Transport of Saharan dust over the Caribbean Islands: Study of an event

R.H. Petit, Michel Legrand, Isabelle Jankowiak, Jack Molinié, Christian Asselin de Beauville, J.L Mansot

► **To cite this version:**

R.H. Petit, Michel Legrand, Isabelle Jankowiak, Jack Molinié, Christian Asselin de Beauville, et al.. Transport of Saharan dust over the Caribbean Islands: Study of an event. Journal of Geophysical Research, 2005, 110 (D18), 10.1029/2004JD004748 . hal-01850178

HAL Id: hal-01850178

<https://hal.univ-antilles.fr/hal-01850178>

Submitted on 12 Feb 2021

HAL is a multi-disciplinary open access archive for the deposit and dissemination of scientific research documents, whether they are published or not. The documents may come from teaching and research institutions in France or abroad, or from public or private research centers.

L'archive ouverte pluridisciplinaire **HAL**, est destinée au dépôt et à la diffusion de documents scientifiques de niveau recherche, publiés ou non, émanant des établissements d'enseignement et de recherche français ou étrangers, des laboratoires publics ou privés.

Transport of Saharan dust over the Caribbean Islands: Study of an event

R. H. Petit,¹ M. Legrand,² I. Jankowiak,² J. Molinié,¹ C. Asselin de Beauville,¹ G. Marion,¹ and J. L. Mansot³

Received 9 March 2004; revised 2 August 2004; accepted 24 August 2004; published 26 April 2005.

[1] A dust plume transported across the Atlantic Ocean from West Africa to Guadeloupe in June 1994 is studied using several complementary and cross-checking techniques. During this event the dust optical depth measured in Guadeloupe was high from 19 to 22 June, peaking at 1. Meteosat-5 IR imagery is used to locate in SW Sahara the source of emitted dust, consistent with the simulated backward trajectories of the dusty air masses arriving over Guadeloupe. Meteosat-3 visible light spectrometer (VIS) imagery over the north tropical Atlantic shows the dust plume leaving the African coast on 15 June and its subsequent spreading over ocean on the following days. The back trajectories indicate a strong uplift from the African source to an altitude of 5000 m on 14 and 15 June, followed by a subsiding motion of the dust plume from the African coast to Guadeloupe, in agreement with the meteorological soundings performed at east and west sides of the Atlantic Ocean. Such uplifts, observed during summer, are shown to be a condition for the long-range transport of dust through the Atlantic. It is also observed that while dust transport is associated with the dynamics of the Saharan air layer, the latter can be dust free. The transported mass of dust was in the range 2.5–5 Mt for this event. Electronic microscopy applied to the mineral particles collected in rainwater just after the dust event shows the predominance of particles larger than 1 μm in the long-range transport from Africa.

Citation: Petit, R. H., M. Legrand, I. Jankowiak, J. Molinié, C. Asselin de Beauville, G. Marion, and J. L. Mansot (2005), Transport of Saharan dust over the Caribbean Islands: Study of an event, *J. Geophys. Res.*, 110, D18S09, doi:10.1029/2004JD004748.

1. Introduction

[2] Important amounts of mineral dust are transported during the period from April to September from their African sources in the Sahara and in the Sahel, to the Caribbean Sea [Prospero *et al.*, 1981]. So they constitute, through their radiative impact and their interaction with clouds, a significant climatic feature of the Antilles. For this reason, we began in 1993 at the Laboratoire de Physique de l'Atmosphère Tropicale, in collaboration with R. Mazurie from the MétéoFrance Center in Guadeloupe, a study on the occurrence of the dust events and on their impact on the local climate [Petit *et al.*, 2001].

[3] Events of Saharan dust arriving over the Caribbean Sea have been previously reported [Carlson and Prospero, 1972; Prospero, 1981a; Karyampudi *et al.*, 1999]. This paper presents different aspects of such an event observed in Guadeloupe, a Lesser Antilles island, French West Indies

(16.2°N, 61.5°W) from 19 to 23 June 1994 (observations reported by MétéoFrance [1994]). This event was chosen for its high turbidity. During dust-free days in Guadeloupe, the visibility at sea level is usually 25–30 km or more and the aerosol optical depth measured at wavelengths of 870 and 1020 nm are never much larger than 0.2. During this 19–23 June dust event, the visibility decreased to 9 km and the aerosol optical depth at 870 nm peaked up to 1. During its occurrence, airplane pilots have reported the presence of a reddish dust layer at altitude.

[4] The data used and the methods applied in this study deal with meteorological observations and measurements (visibility, wind and pressure maps, vertical soundings) and simulations (back trajectories of air masses), ground-based radiometry (supplying photometric measurements of aerosol optical depth), satellite remote sensing of dust (Meteosat visible light spectrometer (VIS) and IR images processing, supplying respectively dust optical depth and an IR dust index), and electronic microscopy (size, shape, and composition of collected dust particles). In section 2, the data and methods are detailed. Section 3 describes the dust event of 19–23 June 1994, under its various aspects. These results allow a comprehensive description of the cycle of a dust event, from its generation in the Sahara to its passage over Guadeloupe, with emphasis on its meteorological background. They are discussed in section 4. The main results of this study can be summarized as follows.

¹Laboratoire de Physique de l'Atmosphère Tropicale, Université Antilles Guyane, Pointe à Pitre, Guadeloupe, French West Indies.

²Laboratoire d'Optique Atmosphérique, Université des Sciences et Technologies de Lille, Villeneuve d'Ascq, France.

³Groupe de Technologie des Surfaces et Interfaces EA 24-32, Université Antilles Guyane, Pointe à Pitre, Guadeloupe, French West Indies.

[5] 1. The dust event of 19–23 June covered most of the north tropical Atlantic during its transport: the transported mass is estimated to 2.5–5 Mt, the supermicronic dust particles collected in Guadeloupe have a typical size of 4 μm .

[6] 2. The source of this dust event, referenced in the literature, is located in a depression of the SW Sahara and NW Sahel.

[7] 3. Dust was emitted from this source on 14 and 15 June and lifted up to 5000 m over Africa, then it underwent a smooth subsiding motion from 5000 to 3200 m during its transport through the Atlantic.

[8] 4. This subsidence is observed to be a regular feature of dust transport through the Atlantic, involving a minimum altitude of 3000 m over the Cape Verde islands for dust to be transported to the Guadeloupe.

[9] 5. The transport over ocean is realized in a Saharan air layer (SAL) bounded by temperature inversions and characterized by typical vertical gradients of potential temperature and of water vapor mixing ratio and by a typical static energy.

[10] 6. Extending the study to the events observed over Guadeloupe and Sal island, shows that dust occurrence is always associated to a SAL, but conversely a SAL is not systematically dusty.

2. Data and Methods

2.1. Meteorological Data

2.1.1. Meteorological Observations in Guadeloupe

[11] At Pole Caraibe Airport (located near Le Raizet, at 2 km from Fouillole where the University of Antilles Guyane stands), MétéoFrance collects observations every 3 hours about the occurrence and importance of dust plumes, the cloudiness of the sky, and the occurrence of rainfall. Human observers also estimate the horizontal visibility at ground level (altitude 8 m) [*MétéoFrance*, 1994].

2.1.2. Meteorological Soundings Over Guadeloupe and Sal

[12] In Guadeloupe, in 1994, soundings were performed by MétéoFrance once a day at 1200 UTC, i.e., at 0800 local standard time (LST). In Sal (16.7°N, 22.9°W), a Cape Verde island 700 km off the West African coast, the Serviço Nacional de Meteorologia e Geofísica (SNMG) performs a daily sounding at 1130 UTC, i.e., at 1030 LST. The soundings supply the vertical profiles of temperature T , pressure p , relative humidity U and wind direction and intensity, from which are derived several relevant parameters.

[13] 1. The partial pressure $e = Ue_s/100$ is derived from the relative humidity $U(\%)$, e_s being the water vapor pressure of saturated air at temperature T . The mixing ratio r (in grams of water vapor per kilogram of dry air) depends on air pressure p and partial pressure e of water vapor according to

$$r = 0.622e/(p - e) \quad (1)$$

[14] 2. The lapse rate dr/dz at different altitudes z is suitable to characterize the vertical structure of the atmosphere.

[15] 3. The dry potential temperature θ is the temperature reached by a particle of dry air at pressure p and temperature T when it is adiabatically carried to the level 1000 hPa

$$\theta = T(p/p_0)^{(1-\gamma)/\gamma} \quad (2)$$

where θ and T are expressed in kelvins and γ is 1.4 for air. The lapse rate $d\theta/dz$ is also considered a useful parameter [*Prospero and Carlson*, 1972]. A constant value of θ in a layer means atmospheric neutral stability in this layer.

[16] 4. The static energy E_s is an index that characterizes the atmospheric stability at level p , taking into account the different thermodynamic processes. It does not vary during an adiabatic transformation

$$E_s(p) = gz + c_p T + Lr \quad (3)$$

It is expressed in kJ kg^{-1} , with $g = 9.8 \text{ m s}^{-2}$, c_p being the air specific heat at a constant pressure, and L being the specific latent heat for water condensation.

[17] The static energy E_s is used to characterize the occurrence of tropical depressions or dry Saharan air masses over Guadeloupe and Sal. Hereafter a depression means either a disturbance (i.e., an event limited to clouds and rainfall), a storm, or a hurricane. From the Barbados Oceanographic and Meteorological Experiment (BOMEX) carried out in the Caribbean Islands, *Aspliden* [1972] deduced that a minimum in the E_s profile is found at a level near 750 hPa. He proposed a correspondence between this minimum of E_s and the mode of convection. In particular, the tropical depressions associated with rainfall are associated in turn with values of E_s higher than 330 kJ kg^{-1} . Thus a threshold of 330 kJ kg^{-1} for the mean static energy between 700 and 800 hPa is used in this study as an index of occurrence of the depressions over Guadeloupe. On the contrary, a Saharan air mass is associated to E_s values lower than 330 kJ kg^{-1} . In the case of Sal, we apply this same criterion with a slight adaptation of the threshold value at 325 kJ kg^{-1} for the mean value of E_s between 850 and 900 hPa.

2.1.3. Meteorological Pressure and Wind Maps

[18] MétéoFrance supplied us with pressure and wind maps at the surface and at 850 and 700 hPa, at 1200 UTC, from 13 to 23 June 1994. They cover a zone from 10°S to 40°N and from 20°E to 90°W. They have been calculated using the model ARPEGE.

2.1.4. Air Mass Back Trajectories Over the North Atlantic Ocean

[19] Six-day back trajectories were calculated by MétéoFrance for air masses reaching Guadeloupe at the levels 850 and 700 hPa (near 1500 and 3200 m), with starting points over Guadeloupe from 19 June at 1200 UTC to 23 June at 0000 UTC at 12-hour intervals. These calculations were made by interpolating wind field reanalyses from the meteorological global model of the European Centre for Medium-Range Weather Forecasts (ECMWF). The model wind field has a horizontal grid step of 1.875° and is given at 6-hour intervals (0000, 0600, 1200, and 1800 UTC). The three components of the wind vector are

Table 1. Calibration Coefficients and Estimated Uncertainties of the Radiometer at the Wavelengths 870 and 1020 nm

	λ , nm	
	870	1020
$\ln V_{0m}$ (Jungfrauoch)	9.687	9.387
$\ln V_{0m}$ (Guadeloupe)	9.65 ± 0.05	9.33 ± 0.05

given for standard levels at 1000, 850, 700, 500, 400, 300, 250, and 200 hPa.

2.2. Photometric Ground-Based Measurements

[20] Sun photometric measurements at the wavelengths $\lambda_1 = 1020$ nm and $\lambda_2 = 870$ nm were carried out at the University of Antilles Guyane from the roof of a building (altitude 30 m) with a hand-held CIMEL photometer. A filtered silicon detector measures the radiance extinction of the direct sunbeam at the wavelength λ . According to Beer's law,

$$V(\lambda) = V_o(\lambda) \exp[-m\delta(\lambda)] \quad (4)$$

where V and V_o are the solar irradiances measured at ground level and at the top of the atmosphere (derived from calibration), respectively, δ is the total atmospheric optical depth, and m is the optical air mass.

[21] The total optical depth δ results from the addition of Rayleigh scattering δ_R , aerosol extinction δ_A and gaseous absorption δ_G . It is computed using the calculated optical air mass m , the photometric measurements V and the value V_o derived from the calibration coefficient of the instrument V_{0m} (i.e., the V_o value for the mean Earth-Sun distance). Then the aerosol optical depth δ_A is derived from δ by subtracting $\delta_R(\lambda)$ and $\delta_G(\lambda)$, which can be calculated with accuracy.

[22] The first source of error with this method is generally due to the determination of V_{0m} and to its evolution especially in connection with the ageing of the filters equipping the instrument. Prior to its use in Guadeloupe, the photometer was calibrated at the Jungfrauoch station (Davos, Switzerland), at an altitude of 3580 m. During the measurements in Guadeloupe, the good stability of the calibration coefficients at 870 and 1020 nm was checked by drawing Langley plots of the photometric data measured during clear days with a weak turbidity. Table 1 shows the calibration coefficients V_{0m} and their estimated uncertainties ΔV_{0m} . The corresponding uncertainty on the aerosol optical depth calculated using (4) is given by

$$\Delta\delta_A = \frac{1}{m} \frac{\Delta V_{0m}}{V_{0m}} \quad (5)$$

this uncertainty is maximum in the middle of the day with a value of 0.05.

[23] The slight effect of the silicon cell temperature on the photometric measurements at 1020 nm has been corrected. The cell temperature varying between 25 and 30°C for the measurements in Guadeloupe, involved a bias never exceeding 5% on the aerosol optical depth. After correction of this temperature effect, the residual error can be neglected.

[24] In order to describe the dependence of the optical depth on the wavelength, we use Ångström's law:

$$\delta_A(\lambda) = \beta\lambda^{-\alpha} \quad (6)$$

where the turbidity parameter β depends upon the aerosol loading of the atmosphere and the Ångström exponent α is a function of the particle size distribution. From the aerosol optical depth values measured at wavelengths λ_1 and λ_2 , we calculate the Ångström exponent α_{1-2} :

$$\alpha_{1-2} = \ln(\delta_A(\lambda_2)/\delta_A(\lambda_1))/\ln(\lambda_1/\lambda_2) \quad (7)$$

2.3. Satellite Tools

[25] Located in the equatorial plane, the geostationary satellites are suitable for observing the dust plumes emitted from Saharan and Sahelian sources and crossing over the tropical Atlantic Ocean, up to the Caribbean islands. Data at 1200 UTC (middle of the day in western Africa) from Meteosat-5 located above the Gulf of Guinea at the Greenwich meridian are used for the study of dust emission and transport above the African continent. The (IR) images of the thermal infrared channel (10.5–12.5 μm) are processed so as to reveal the dust patterns over Africa.

[26] During the studied event, Meteosat-3 was moved from its nominal location above the Gulf of Guinea to 75°W in order to compensate for a temporary lack of data from Goes-East. From this location, its (VIS) imagery at 1800 UTC in the visible and near-infrared parts of the solar spectrum (0.4–1.1 μm), corresponding to a central wavelength of 640 nm, is processed in order to view the dust transport from the African coast to the Caribbean islands.

2.3.1. VIS Channel Processing

[27] Daily Meteosat-3 images are obtained in the full resolution format. The images cover the area extending from the African coast to the Caribbean Islands, within a zone between 2°N and 23°N. The resolution for the VIS channel is (2.5 \times 2.5) km² at the nadir. In order to exclude data with sunglint conditions, we used images at 1800 UTC (1400 LST, in Guadeloupe). In the VIS satellite imagery, the ocean surface is dark and the presence of dust increases the upward radiance of sunlight by scattering processes in the aerosol layer. *Jankowiak and Tanré* [1992] described the method used to obtain dust optical depth from Meteosat VIS data.

[28] In a first step, we have to create a reference scene corresponding to a molecular atmosphere (free of any aerosol). Assuming an open ocean reflectance and a tropical atmosphere model, we compute a mean monthly reference image.

[29] In a second step, we eliminate clouds by using a method based on the spatial coherence concept. The cloud-covered areas over ocean show a greater spatial variance than the cloud-free ones. Hence we identify the cloudy pixels by comparing the computed standard deviation σ_c of the radiometric level for 3 \times 3 pixel squares, to a threshold value of 4 counts. In addition, to be sure to eliminate some thick uniform clouds, a second threshold of 50 counts for the pixel radiometric level C is applied [*Jankowiak and Tanré*, 1992]. So, a pixel is declared cloudy if it is at the

center of a 3×3 pixel square with $\sigma_c > 4$ counts, or if $C > 50$ counts.

[30] In a last step, the aerosol optical depth values are derived from the comparison of the satellite image (after cloud masking) with the reference image, an aerosol model being selected.

2.3.2. IR Channel Processing

[31] Around midday, the presence of desert dust over arid African areas, results first in a decrease of solar irradiance at the Earth surface and hence in a temperature drop of the land surface. So, the ground-emitted thermal infrared radiance is weakened. In addition the dust layer is much colder than the overheated underlying surface, so that the upwelling radiance is attenuated through the dust layer. These two additive effects are responsible for large drops of the thermal infrared radiance outgoing to space, and of the corresponding brightness temperature [Legrand *et al.*, 1992]. This effect is applied to the remote sensing of desert dust over Africa using the IR channel of the Meteosat satellites. The Meteosat IR images at 1200 UTC are processed as follows in order to derive a parameter indicating the presence of dust, referred to as the Infrared Difference Dust Index (IDDI) [Legrand *et al.*, 2001]:

[32] 1. The raw satellite data are corrected for day-to-day variations of the IR channel sensitivity, using the calibration on board.

[33] 2. Ideally, these corrected data should be compared to data from a cloud- and dust-free atmosphere. Practically, a reference image (RI) is obtained by selecting the highest radiance values for every pixel, from a daily series of Meteosat IR images, half a month long. In this composite RI, clouds and dust are eliminated as strictly as possible: only the permanent information about surface has been retained.

[34] 3. The variable atmospheric elements: clouds and dust, are separated from the land surface by subtracting each initial corrected image from the RI, resulting in a difference image (DI).

[35] 4. The clouds are identified in the DI by means of an algorithm related to the spatial coherence method of Coakley and Bretherton [1982]. They are then masked, and only the cloud-free structures, constituting the IDDI, are kept.

2.4. Electron Microscopy

2.4.1. Samples Preparation

[36] Samples of rainwater were collected at Sainte Anne, at 15 km from the University of Antilles Guyane, and near Pole Caraïbe Airport. They were then prepared for Transmission Electron Microscopy (TEM) examination. The rainwater (50 cm^3) is first centrifuged at 2000 rpm during 10 min. The water was eliminated and the remaining solid particles were ultrasonically dispersed into one cubic centimeter of pure ethanol. A drop of this dispersion was then deposited onto a perforated carbon film supported on a copper grid. After evaporation of the solvent, the solid particles are stuck onto the carbon film by Van der Waals interactions. The sample was then examined by a microscope.

2.4.2. Experimental Conditions

[37] The TEM examinations were carried out on a H8000 Hitachi microscope, equipped with an ISIS Energy

Dispersive X-ray Spectrometer (EDXS), running at 200 kV with a LaB₆ cathode. The morphology and structure of the particles were investigated in a TEM mode (bright field imaging and selected area diffraction (SAD)) whereas chemical analyses (EDXS) were carried out in scanning transmission electron microscopy (STEM). The chemical and structural heterogeneity of some particles was revealed by X-ray mapping records.

3. Study of the Dust Plume of 14–23 June 1994

[38] During the wet season of 1994, several dust events were observed over Guadeloupe. The dust plume emitted on 14 June in Africa and leaving Guadeloupe on 23 June was characterized by particularly high values of optical depth, along with other characteristics typical of dust plumes observed during the wet season in the Caribbean Islands.

3.1. Meteorological Situation Over the Tropical Atlantic (Trade Winds and Easterly Waves)

[39] The wet season, called “hivernage” in the French West Indies, begins in June and lasts 5 months. During this season, low-pressure zones called easterly waves regularly affect the islands, resulting in disturbed weather. The mean interval between two depressions is about a week. In June 1994, four tropical depressions were observed in Guadeloupe, on 5, 16, 25 June and during the night between 28 and 29 June, after their crossing of the Atlantic Ocean [MétéoFrance, 1994].

[40] The wind regime over the ocean is characterized by the easterly trades, with some fluctuations resulting from the passage of easterly waves [Triplet and Roche, 1971; Molinié, 1991]. This wind direction is determined by the two anticyclones of the Azores and of the Bermudas which merge during the wet season. At these latitudes the direction of the wind changes at high altitudes (above 6000 m) where it blows from west, northwest or southwest [Triplet and Roche, 1971].

[41] Over the ocean, the meteorological maps from MétéoFrance show east winds in the lower troposphere during the entire period from 13 to 23 June. This is illustrated in Figures 1a and 1b showing the maps for 18 June at 1200 UTC, with the wind speed and direction and the contour lines at 850 hPa. The high pressures, associated with sunny weather, are bounded by the 1560 m contour line. The mean value of the wind velocity at this level is 10 m s^{-1} , indicating that the air masses will cover in about 4–5 days the distance of 4000 km separating the West African coast from the Lesser Antilles.

[42] Over Africa, pressure maps at 10 m show a deep depression zone (1006 hPa), located between 3°W and 20°E and between 15°N and 25°N on 14 June at 1200 UTC. The corresponding wind map shows that the maximum velocity of the surface wind exceeds 10 m s^{-1} in Mali, near 20°N and 5°W . This is shown in Figures 2a and 2b, derived from the surface maps supplied by MétéoFrance.

3.2. Satellite Images of the Dust Plume Genesis

[43] In Figure 3, IDDI images display the dust patterns over West Africa at 1200 UTC, on 14 and 15 June 1994. On 14 June, a dust plume is visible in the SW Sahara and NW Sahel. It is associated to the depression zone observed over

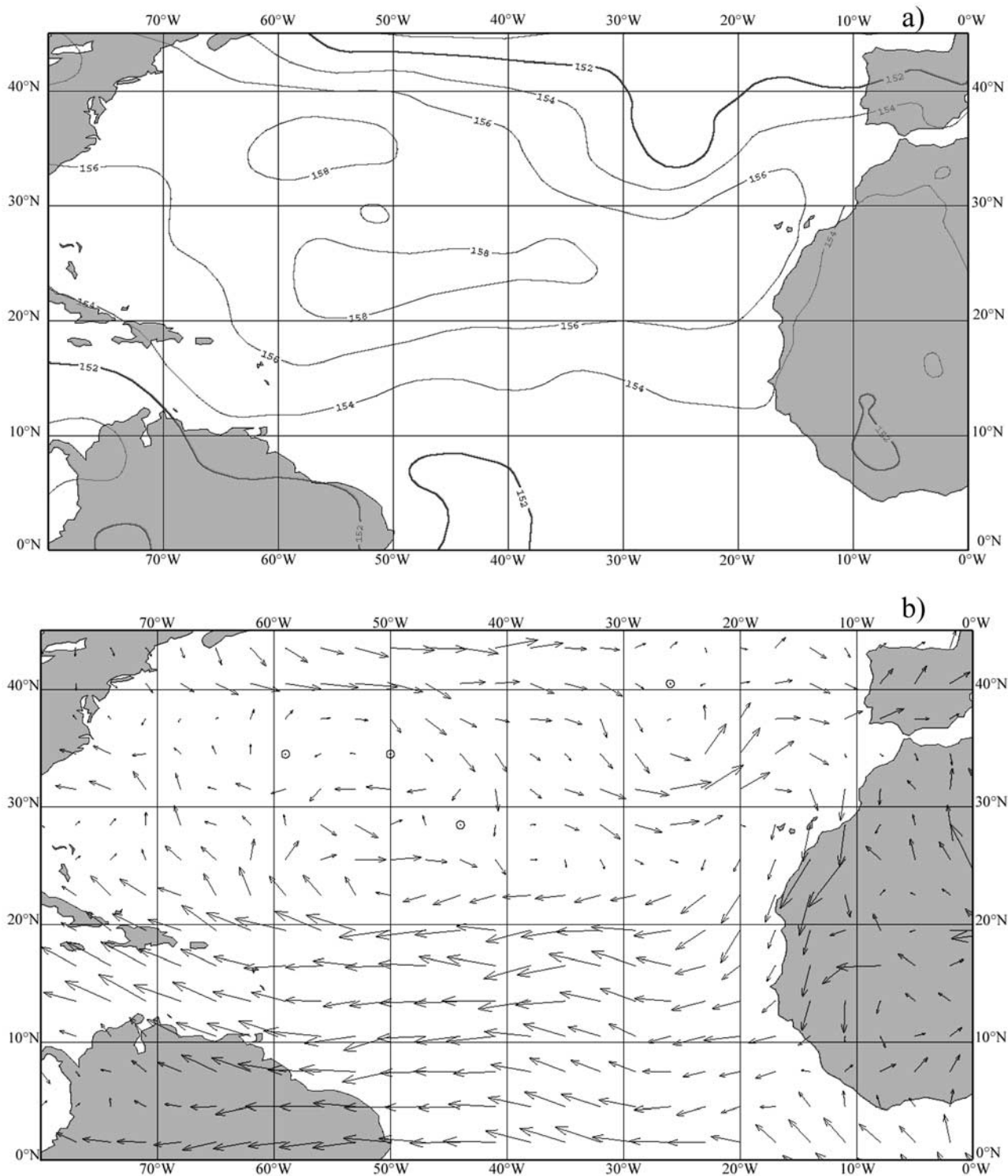


Figure 1. Maps at 850 hPa of the winds over the Atlantic Ocean on 18 June 1994 at 1200 UTC (from MétéoFrance): (a) pressure and (b) wind.

West Africa in Figure 2a. The limit between yellow and green (underlined with a dashed line), corresponding to an IDDI value of 8 K, delineates a dust front according to a quasi-straight direction from SE Algeria (27°N, 2°W) to Mauritania (17°N, 12°W). The dust plume spreads SE of this line, over Algeria, Mali, and Mauritania. The IDDI

peaks around 22°N, 3°W (black square), at a value close to 18 K, corresponding to an aerosol optical depth comprised between 1.5 and 4.5, according to *Legrand et al.* [2001]. The area with high IDDI values matches with sources very active in this period of the year [see *Brooks and Legrand*, 2000, Figure 4]. It corresponds to erodible soils, close to a

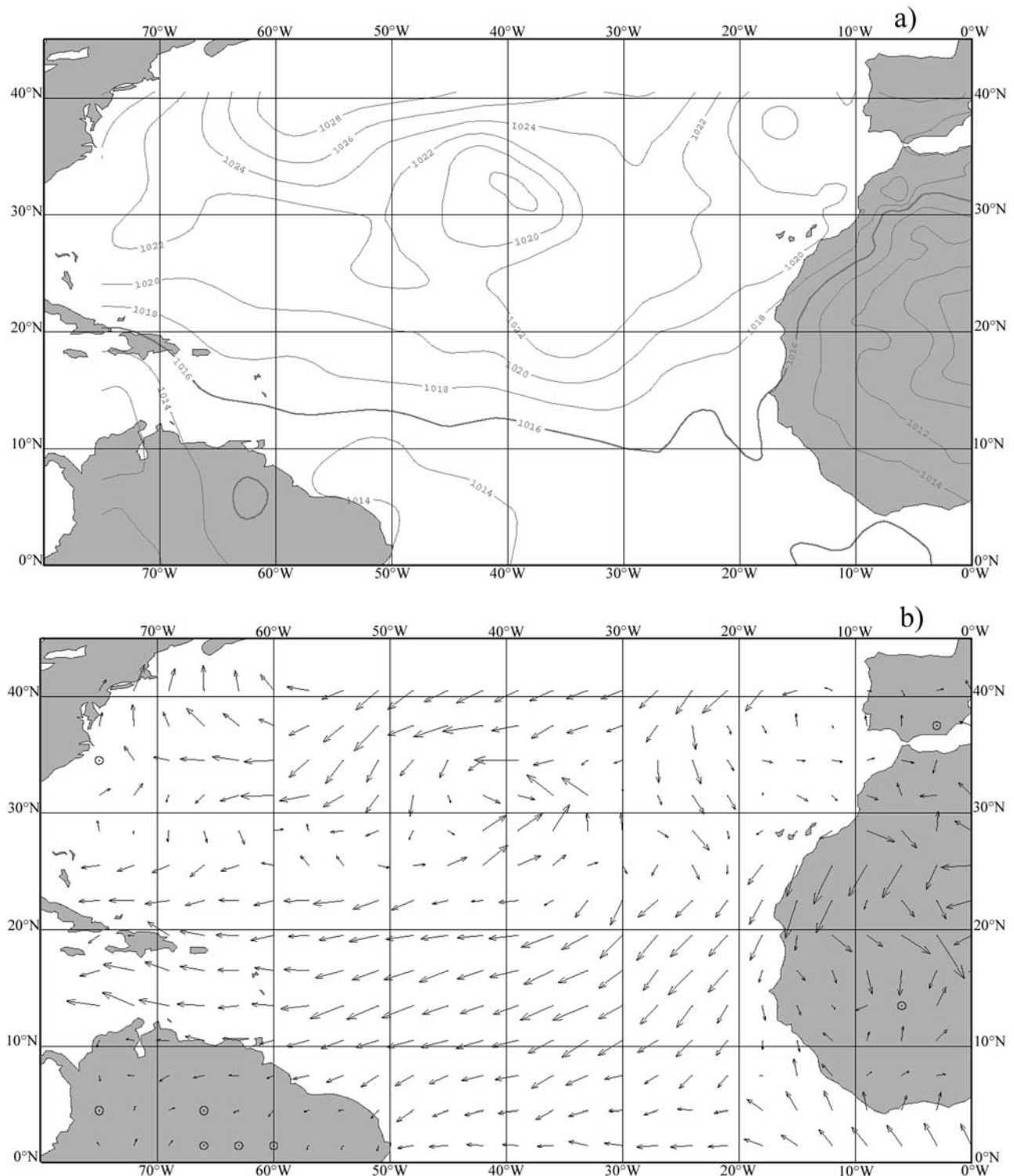
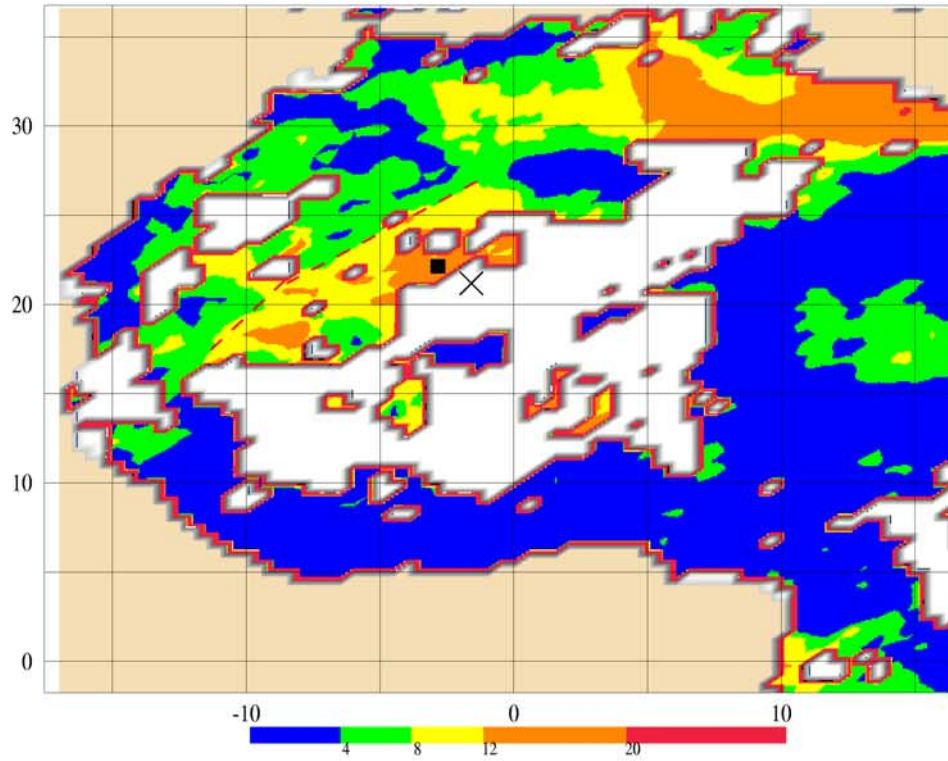


Figure 2. Surface maps on 14 June 1994 at 1200 UTC (from MétéoFrance): (a) pressure and (b) wind.

dry salty lake in the northern Mali (saltpan of Taoudenni). The erodible surfaces in this region are characterized by a moderately low wind speed threshold of dust emission of $7\text{--}8\text{ m s}^{-1}$ at the height of 10 m [see *Marticorena et al.*, 1997, Plate 1]. Hence this is certainly the location of the source of the dust plume, since the surface wind speed at 10 m exceeded then 10 m s^{-1} in this region (Figure 2b).

The full extent of the dust plume cannot be determined because of an extensive cloud cluster covering large parts of the Sahara and of the Sahel. However, at this stage the plume is far inland and no dust is observed crossing the Atlantic coast. In the top right corner of Figure 3 (14 June), a second thick dust plume can also be seen above Libya, Tunisia, and Algeria, near the Mediterranean coast.

14 June 1994



15 June 1994

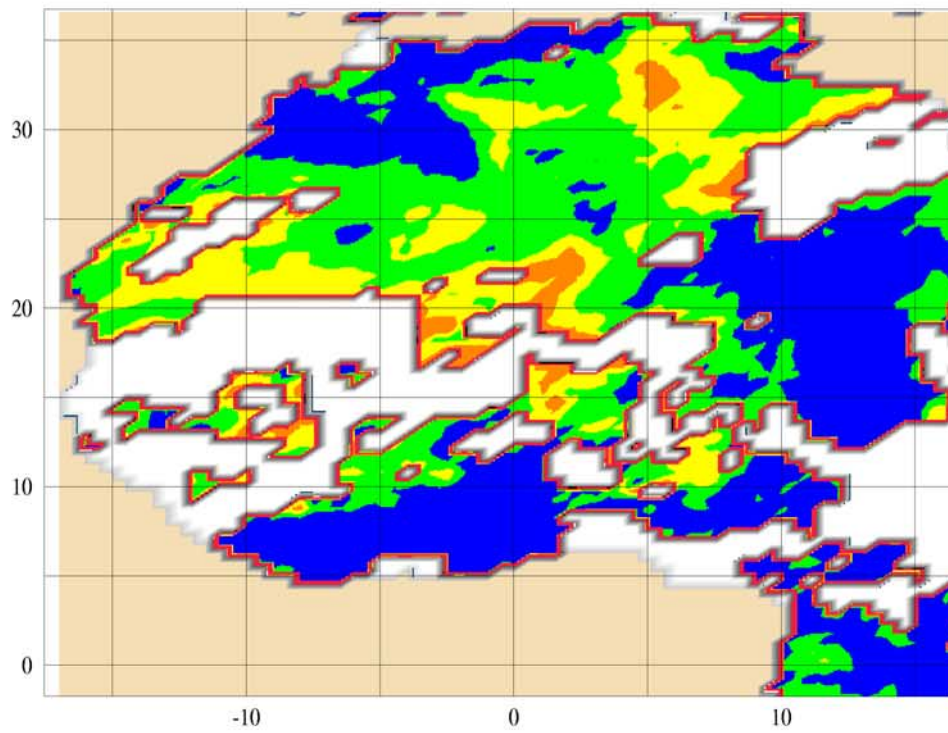


Figure 3

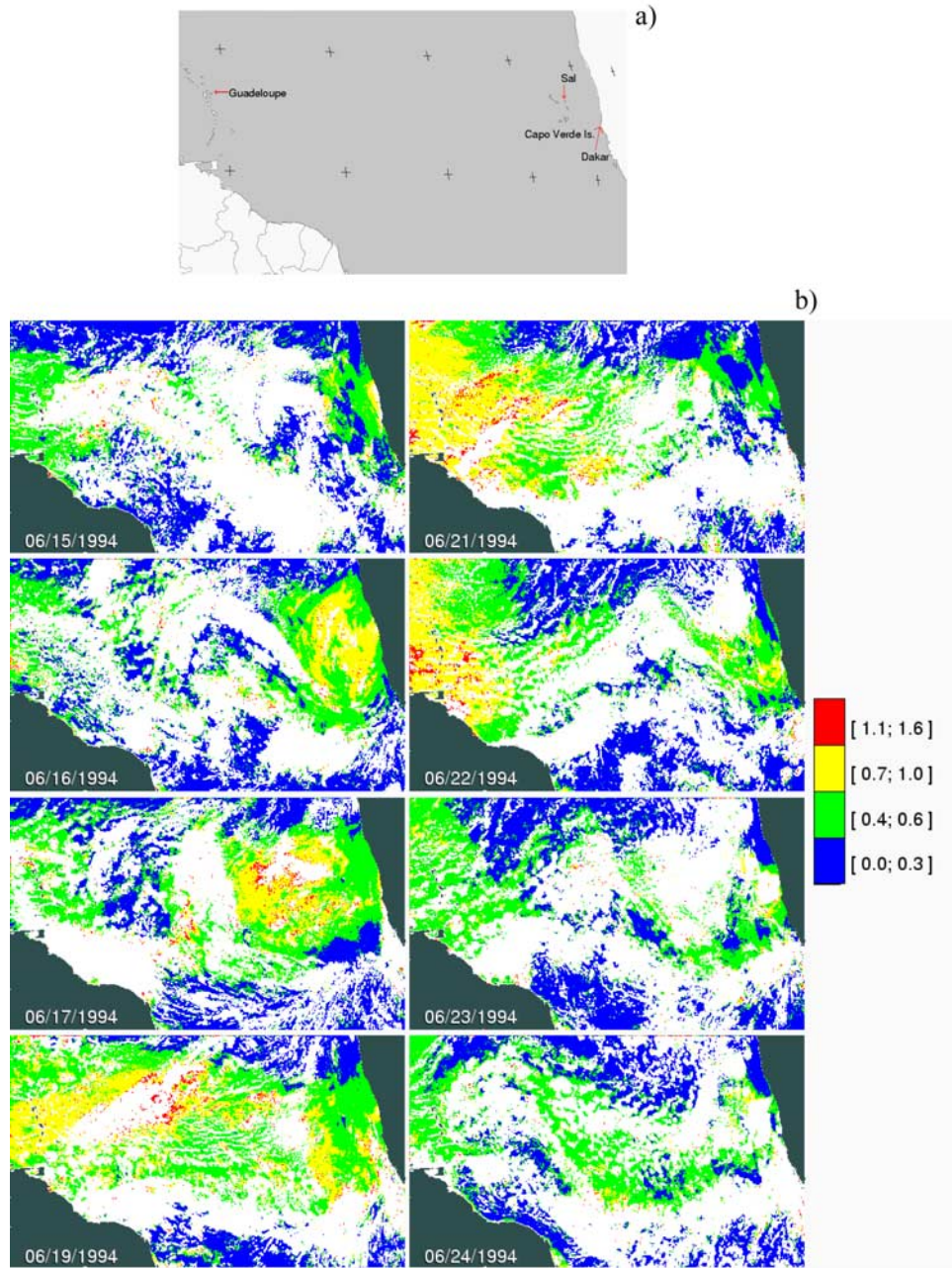


Figure 4. (a) Geographical area observed by Meteosat-3, presented in Figure 4b. The crosses indicate the latitude belt between 10°N and 20°N , from 20°W to 60°W . (b) Daily aerosol optical depth over the Atlantic Ocean in June 1994 at 1800 UTC, obtained from VIS images of the satellite Meteosat-3 (full resolution) located at 75°W (Msphinx images). Images must be read from top to bottom and from left to right. A black mask covers the South American and the African continents. The color scales increasing aerosol optical depth values from blue to red. The clouds are replaced by a white mask.

Figure 3. Dust distribution over West Africa (0° – 35°N , 16°W – 15°E) on 14 and 15 June 1994 at 1200 UTC, by means of the Infrared Difference Dust Index (IDDI) derived from Meteosat-5 IR (Mgraph images). The IDDI is expressed as a brightness temperature drop for pixels $1/2^{\circ} \times 1/2^{\circ}$ of resolution. The color scale shows IDDI values (K), increasing from blue to red. The clouds are replaced by a white mask. The cross located around 20.5°N and 2.5°W on 14 June, spots the air masses close to the ground surface which will be over Guadeloupe at 3200 m on 20 June 1994, at 1200 UTC (from the back trajectory BT3200).

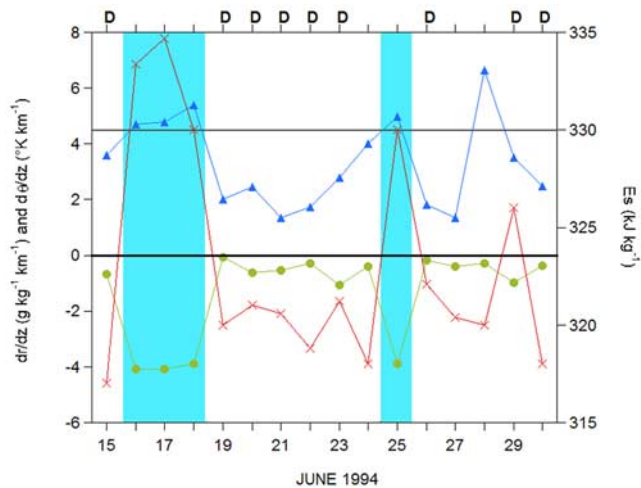


Figure 5. Time evolution of the following parameters from 15 to 30 June 1994, over Guadeloupe: dr/dz (in $\text{g kg}^{-1} \text{km}^{-1}$) (circles, yellow), vertical gradient of r between 2000 and 4500 m; $d\theta/dz$ (in $^{\circ}\text{C km}^{-1}$) (triangles, blue), vertical gradient of the potential temperature θ between 2000 and 4500 m; E_s (in kJ kg^{-1}) (crosses, red), mean static energy between 700 and 800 hPa. These parameters are deduced from the meteorological soundings; D is parameter of dust presence from MétéoFrance surface observations. Low-level T inversion days (from the soundings) are identified by cyan stripes.

It is not joined to the previous plume, as confirmed by the image of 15 June.

[44] On 15 June, while emission continues inland, the dust plume has moved westward and reached the Atlantic coast. Dust is now being transported over the ocean, as proved by the VIS image for the same day in Figure 4b, 6 hours later. Considering the estimated IDDI- δ_A conversion proposed by Legrand *et al.* [2001], the values of δ_A along the coast in the area of expelling are between 0.7 and 2. However, only the coasts of Morocco and north Mauritania are cloud free. Clouds prevent the dust pattern from being described farther south.

3.3. Satellite Images of the Dust Transport Over the Tropical Atlantic

[45] To obtain the satellite dust optical depth over ocean, we have compared several background mineral dust models. The background model of Shettle [1984] associated with a complex index of $(1.53 - 0.008i)$ at 640 nm provides a good agreement with the photometric optical depth measured at Guadeloupe.

[46] Figure 4a shows the geographical region of dust transport, covered by Meteosat-3. Figure 4b represents maps of aerosol optical depth derived from Meteosat-3 VIS imagery, over the Atlantic Ocean, at 1800 UTC, from 15 to 24 June 1994 (for 18 and 20 June, images are missing). The large expanse of the studied plume and its intensity are to be noted.

[47] On 15 June, we see near Dakar (Figure 4) the front of the expelled dust plume, in agreement with the IR image at 1200 UTC for the same day (Figure 3). Then the maximum optical depth along the coast is larger than 0.6 (yellow

color). On 16 June, the dust plume exceeds the area between 10 and 20°N and from the African coast to 30°W, with an optical depth always higher than 0.6 (yellow color) and peaking over 1 (red color). On 17 June, the plume is 1000 km farther westward, and most of it is west of the Cape Verde islands. From 16 to 19 June, the weather over Sal is very dusty. On 19 June, the plume covers the entire north tropical Atlantic zone and reaches the West Indies. The image of 23 June shows the plume as it leaves Guadeloupe. We notice a second weaker expulsion of aerosol beginning on 22 June over the region of Dakar.

3.4. Aerosol Optical Depth and Horizontal Visibility Over Guadeloupe

[48] Observations of dust presence over Guadeloupe [MétéoFrance, 1994] are presented in Figure 5 for the period 15 to 30 June 1994. Airplane pilots reported the presence over the West Indies islands of a thick red dust layer above 1500 m from 19 to 23 June. The aerosol optical depths deduced from photometric ground-based measurements at $\lambda = 870 \text{ nm}$ over Guadeloupe, and from Meteosat-3 VIS images over the ocean (averaged over 400 pixels in the vicinity of the island), are shown in Figure 6 from 15 to 30 June. The dust optical depth from Meteosat VIS images [Jankowiak and Tanré, 1992] retrieved using the background desert aerosol model of Shettle [1984] is in agreement with the photometric measurements (Figure 6). During the dust event, when δ_A is high, its dependence with the wavelength vanishes and the Ångström exponent α_{1-2} (shown in Figure 6) is close to zero.

[49] During the period from 19 to 23 June, a high turbidity was observed at ground level in Guadeloupe. The visibility dropped to 9–10 km, instead of the 30 km typical of dust-free days in this season. On 23 and 24 June, the satellite images of Figure 4b show that there is no more

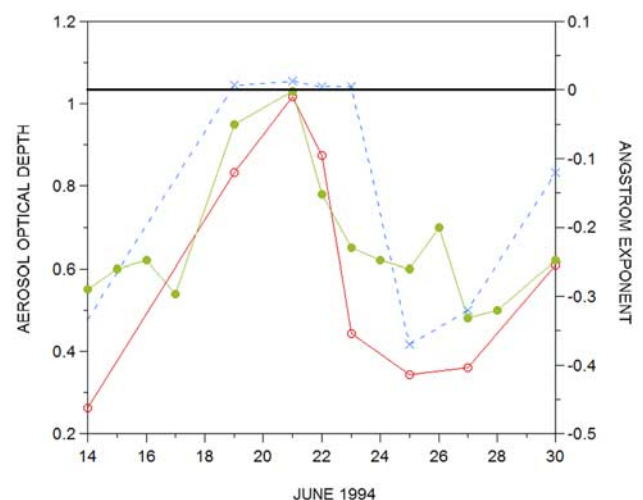


Figure 6. Aerosol optical depth at 870 nm calculated from photometric ground-based measurements in Guadeloupe at 1400 LST (open circle, solid red line); aerosol optical depth from simultaneous (1800 UTC) Meteosat-3 VIS images (solid circle, solid yellow line); Ångström exponent derived from the photometric measurements at 870 and 1020 nm (cross, dashed blue line).

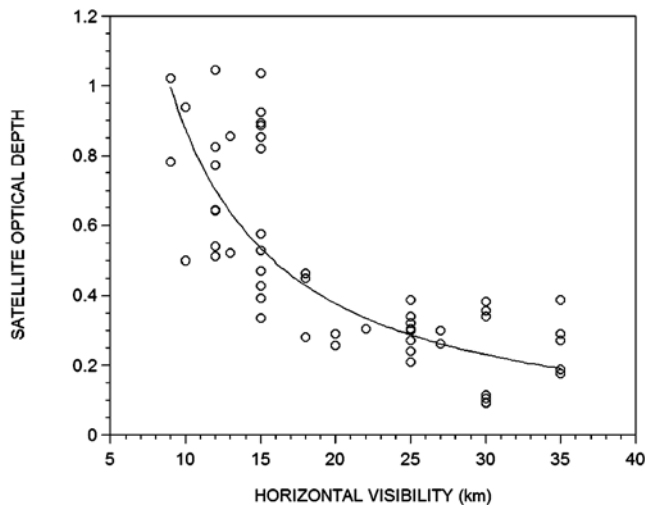


Figure 7. Aerosol optical depth δ_A from Meteosat-3 VIS images as a function of the horizontal visibility measured by MétéoFrance in Guadeloupe, in June 1994.

arrival of dust over Guadeloupe. Then, the visibility has increased to 15–20 km and the aerosol optical depth has decreased to 0.6 according to the satellite and 0.4 according to the photometer, showing that dust is still present in the

atmosphere. As a matter of fact, there were during these 2-day rainfalls of limited intensity, associated to small clouds cells a few kilometers large, which could have realized the scavenging of a part of the dust.

[50] In Figure 7, we can check that the aerosol optical depth (deduced from satellite images), increases when the surface visibility decreases. A curve is fitted using a regression according to a power law

$$\delta_A = 14.5 V^{-1.2} \quad (8)$$

with a correlation characterized by $r^2 = 0.77$.

3.5. Soundings Over Guadeloupe and Sal

3.5.1. Over Guadeloupe

[51] The meteorological soundings in Guadeloupe are drastically different during the dust event, between 19 and 23 June, and outside it. During the dust event, the vertical profiles of the mixing ratio r and of thermodynamic and potential temperatures T and θ respectively, are similar (compare Figures 8b and 8c). They differ from the corresponding vertical profiles before this event (Figure 8a) and after it (Figure 8d) which are similar. Analyzing the period from 15 to 30 June, we can discriminate between the two previous types of profiles according to the value of the static energy E_s in the layer between 700 and 800 hPa.

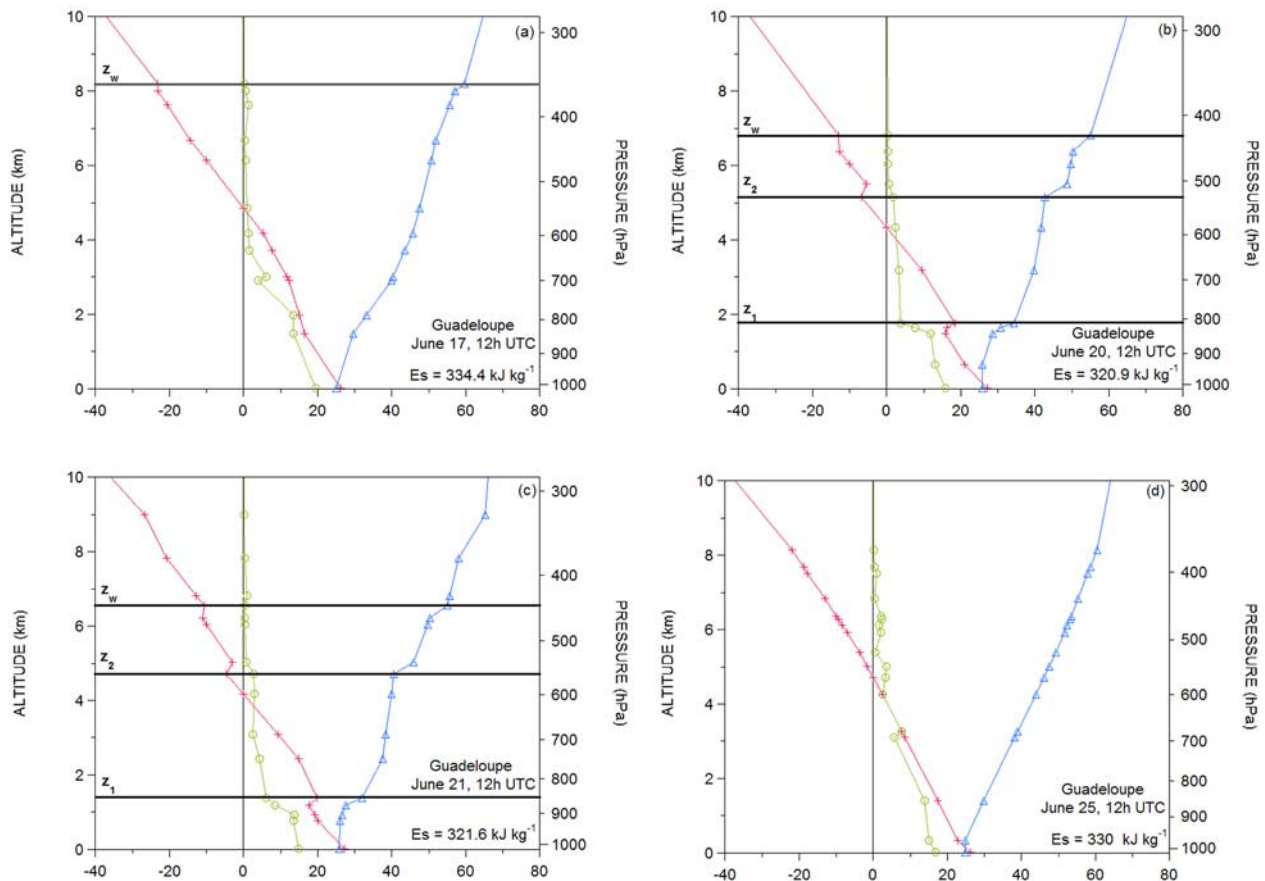


Figure 8. Vertical profiles over Guadeloupe of temperature T in $^{\circ}\text{C}$ (pluses, red), mixing ratio r in g kg^{-1} (circles, yellow), and potential temperature θ in $^{\circ}\text{C}$ (triangles, blue), from the meteorological radio soundings at 1200 UTC (0800 LST): (a) on 17 June, before dust arrival; (b) on 20 June, on a dusty day; (c) on 21 June, a dusty day; and (d) on 25 June, after dust disappeared.

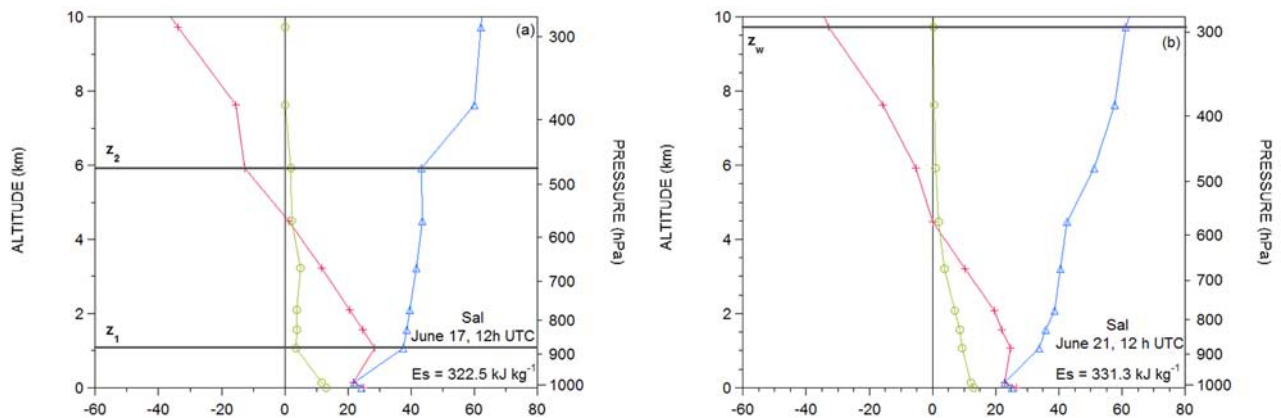


Figure 9. Vertical profiles over Sal of temperature T in $^{\circ}\text{C}$ (pluses, red), mixing ratio r in g kg^{-1} (circles, yellow), and potential temperature θ in $^{\circ}\text{C}$ (triangles, blue), from the meteorological radio soundings at 1030 LST: (a) on 17 June, a dusty day; and (b) on 21 June, after dust disappeared.

[52] 1. When E_s is lower than 330 kJ kg^{-1} , we are in a sunny period, between two tropical disturbances (e.g., the period from 19 to 24 June as shown in Figure 5). Then we observe the presence of a temperature inversion at a low-altitude z_1 (near 1500–2000 m on 20 and 21 June, according to Figures 8b and 8c). In the layer above z_1 , the vertical gradients for the mixing ratio r and the potential temperature θ are close to zero (with $r = 3 \text{ g kg}^{-1}$ and $\theta = 40^{\circ}\text{C}$ on 20 and 21 June). This layer is limited at its top by another (weaker) temperature inversion at a level z_2 (near 5000 m on 20 and 21 June). Above z_2 the air is drier with a mixing ratio decreasing to values as low as 0.1 g kg^{-1} , and the lapse rate of potential temperature increases. These days where z_1 is observed are referred to as low-level T inversion days in the following. They are signaled with cyan stripes in Figure 5, and we can see that all the dusty days are low-level T inversion days.

[53] 2. When E_s reaches or exceeds 330 kJ kg^{-1} , we are in a tropical disturbance (e.g., on 16 to 18 June as shown in Figure 5). The levels z_1 and z_2 and the layer in between have disappeared (see Figures 8a and 8d). The mean vertical gradients calculated for r and θ in the layer between 2000 and 4500 m (altitudes close to the inversion levels z_1 and z_2) show larger absolute values than with low-level T inversion days (Figure 5).

[54] It should be noted that during the night from 28 to 29 June, a disturbance crossed over Guadeloupe [MétéoFrance, 1994], explaining the increased gradient of potential temperature and the corresponding increase of E_s shown in Figure 5. These two types of profiles have been described by Carlson and Prospero [1972].

[55] On Figures 8a, 8b, and 8c, an extra temperature inversion is observed at levels z_w between 6000 and 8000 m, corresponding to a wind direction inversion. On Figure 8d, z_w is above 10,000 m.

3.5.2. Over Sal

[56] The overall characteristics of the atmospheric profiles at Guadeloupe and at Sal, during and outside a tropical depression, show large similarities and some minor differences. At both sites, the atmospheric profiles can be classified by means of the static energy method, into low-level T inversion profiles between two depres-

sions, and profiles without low-level T inversion during a depression.

[57] Similar to the soundings of Guadeloupe, two types of profiles of temperature and mixing ratio appear in the soundings of June 1994 at Sal (Figures 9a and 9b). We can again use the static energy E_s to distinguish between two types of profiles. However, the level of the minimum for E_s is lower over Sal (850–900 hPa), than over Guadeloupe (700–800 hPa). This is related to the low inversion altitude z_1 which increases from 1000 m at Sal to 1500–2000 m over Guadeloupe. This difference results from the warmer sea surface in the Caribbean Sea than near the Cape Verde islands. It arises from heat transport in the oceanic masses [D’Honneur, 1979], and it is responsible for an increased westward height of convection. Moreover the value 330 kJ kg^{-1} at the level 750 hPa adopted for Guadeloupe, has to be slightly modified to 325 kJ kg^{-1} at the level 850 hPa for Sal Island. With this criterion, the soundings of Sal indicate tropical depressions on 1, 12, 14–15, and 21 June (Figure 10).

[58] 1. When E_s is lower than 325 kJ kg^{-1} (Figure 9a), we clearly observe the presence of a strong T inversion at a very low level z_1 . On 17 June, it is characterized by an increase of T of 7 K between 200 and 1000 m. On those days without depression, the vertical gradient for r above the inversion level is very weak (r is nearly constant at 3 g kg^{-1} above 1000 m on 17 June). Above 6000 m, r decreases to very low values (0.1 g kg^{-1}), indicating the level z_2 at 6000 m (Figure 9a). By analogy with the analysis of the soundings of Guadeloupe, these days are referred to as low-level T inversion days. They are indicated in Figure 10 by cyan stripes. Using satellite images, we conclude that all dusty days over Sal are low-level T inversion days (as over Guadeloupe).

[59] 2. When E_s reaches or exceeds 325 kJ kg^{-1} (e.g., on 21 June shown in Figure 9b), a low-level temperature inversion is still visible, but it is very weak (the temperature increase of the inversion is close to zero on 21 June). Over this inversion level, a wet layer indicates the presence of a tropical easterly wave. Such a layer can be characterized by a strong negative gradient dr/dz between 1000 and 6000 m. These days compare well to the days with no low-level T

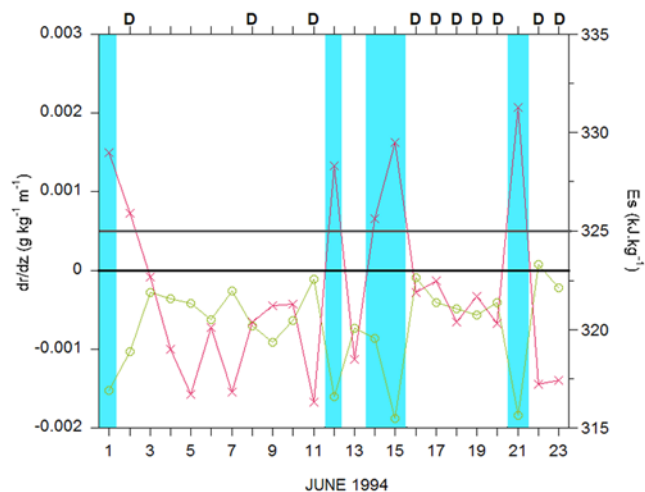


Figure 10. Time evolution of the following parameters from 1 to 23 June 1994, over Sal: dr/dz (in $\text{g kg}^{-1} \text{km}^{-1}$) (circles, yellow), vertical gradient of r between 1000 and 6000 m deduced from the meteorological sounding of the day; E_s (in kJ kg^{-1}) (crosses, red), mean static energy between 700 and 800 hPa. D is parameter of dust presence. Low-level T inversion days are identified by cyan stripes.

inversion in Guadeloupe (Figures 8a and 8d). A weak low-level T inversion persists, however, because of the continental influence on Sal, 700 km off African coast. On the other hand, the profiles of potential temperature keep nearly steady for all the days of June 1994.

3.6. Calculated Backward Trajectories of Dust Over the Ocean

[60] Figures 11a and 11b show 6-day back trajectories of the air masses passing over Guadeloupe on 20 June 1994, at

1200 UTC (0800 LST) at the levels 850 hPa (near 1500 m) and 700 hPa (near 3200 m), respectively called BT1500 and BT3200 hereafter. As demonstrated by the following description, there is evidence that the air masses of BT3200 were dusty when leaving Africa, not for the air masses of BT1500.

[61] In Figure 11a, we see that BT3200 starts on 14 June at 1200 UTC near the level 600 m, in the boundary layer. We locate the point of departure of the associated air mass in northern Mali, near 3°W and 20°N , in a dusty region on this day according to Figure 3. The air masses are then transported westward over the African continent, moving across Mauritania with an ascending motion of 3500 m d^{-1} , up to 5000 m (Figure 11b). They leave Africa on 16 June between 0000 and 0600 UTC, and the same day at 1800 UTC, they are over Sal at the level 4750 m. This is to be compared with the satellite image of 16 June at 1200 UTC (Figure 4b) showing the presence of the dust plume over Sal, and with Figure 10 showing a low-level T inversion at the same time (on 15 June at 1200 UTC, there is no dust presence at Sal, from both the satellite and the sounding). The oceanic trajectory of BT3200 goes directly west between 15°N and 20°N from the African coast to Guadeloupe. There, the altitude of the air masses regularly decreases by $340 \pm 20 \text{ m d}^{-1}$ (Figure 11b).

[62] On Figure 11a, BT1500 starts on 14 June at 1200 UTC over Dakar at an altitude of 3800 m. Then, no dust is observed in this region (Figure 3). The air masses pass over Sal at the 2950 m level on 15 June at 0600 UTC (Figure 11b), before the arrival of dust as shown in Figure 4b, and in agreement with Figure 10 showing no low-level T inversion this day. The trajectory BT1500 over the Atlantic Ocean, between 15°N and 20°N , is similar to BT3200, showing a sinking motion with the same daily decrease of altitude but the air masses are slower and at lower altitudes. So the air masses associated

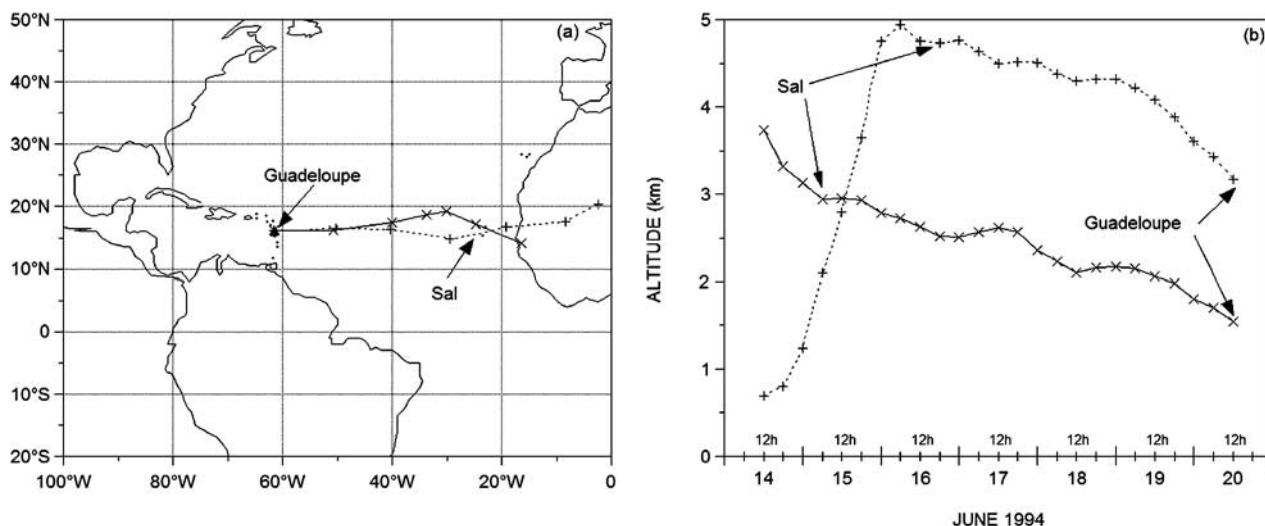


Figure 11. Backward 6-day trajectories of dusty air masses starting from Guadeloupe on 20 June 1994 at 1200 UTC (0800 LST) at levels 700 hPa (BT3200) (pluses) and 850 hPa (BT1500) (crosses). (a) Horizontal profiles. The axes are graduated in degrees, two successive crosses on the trajectories correspond to a day. (b) Vertical profiles, date (June 1994) on x axis, altitude on y axis. Two successive crosses on the trajectories correspond to 6 hours.

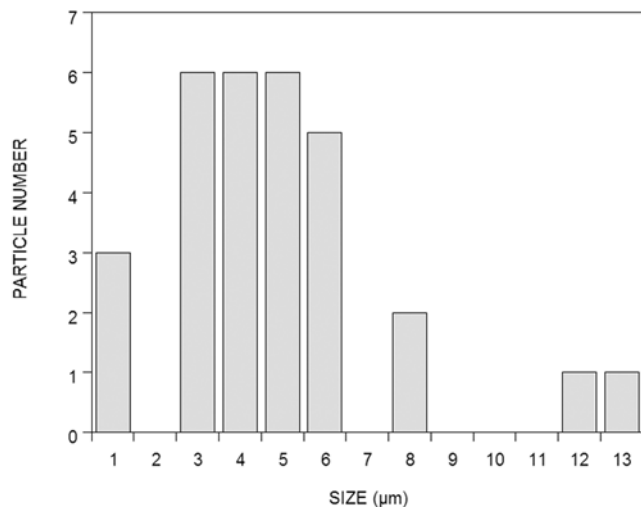


Figure 12. Size distribution of the particles collected from the sample of wet deposit, derived from their observation by transmission electron microscopy.

with BT1500 and BT3200 arrive in Guadeloupe simultaneously, but the former are below the inversion level at 1800 m (Figure 8b) while the latter are above.

[63] All the backward trajectories arriving in Guadeloupe from 19 to 23 June are similar to those shown in Figures 11a and 11b. They show the same downward motion of about 340 m d^{-1} after they left the African coast.

[64] We have used the back trajectories from the Hysplit model supplied by the NOAA (available at <http://www.arl.noaa.gov/ready/hysplit4.html>). These back trajectories show a fair agreement with those from MétéoFrance presented in Figure 11 (particularly with regard to the initial ascending motion of BT3200 and to the subsiding motions over the ocean).

3.7. Structure, Size Distribution, and Composition of the Particles

[65] A rain sample was collected during the night between 23 and 24 June 1994 at Sainte-Anne (15 km far from the University of Antilles Guyane), during the first rainfall after the dust event over Guadeloupe. A second rain sample was collected in the morning of 24 June near Pole Caraibe Airport (2 km far from the University of Antilles Guyane). Because of the preparation in which water is totally eliminated, the collected particles are free of water-soluble minerals such as sea salt and sulfates, usually observed in aerosols collected near the ocean. Comparing the number of particles deposited in the same conditions on the perforated carbon films, the first sample contains a greater amount of insoluble particles than the second one, emphasizing the scavenging effect due principally to the rain wash.

[66] About 30 particles were chemically and morphologically studied. The apparent size (the largest size) of most of the considered particles (25/30) lies in the range 1–8 μm (Figure 12). The modal size is 4 μm . Few submicronic particles (3/30) have been observed with the microscope. Such particles have been perhaps lost when preparing the sample, the grid holes being squares of 0.3 μm side. It is

also possible that the lightest ones have stayed in suspension in the collected rain water while centrifuging.

[67] From a structural point of view, most of the particles are crystalline. All large particles are monocrystalline with the same chemical analysis (this suggests that the preparation does not induce aggregations of small particles). They generally appear as flat particles, which allows them to be observed by transmission. They are mainly constituted of Al, Si, O as major elements and K, Fe, Mg as minor ones, indicating aluminosilicate minerals: feldspar (Figure 13) and clay (Figure 14).

4. Discussion of Dust Transport

4.1. The Saharan Air Layer (SAL)

[68] *Carlson and Prospero* [1972] attributed the existence of the low-altitude temperature inversion to the presence of dry and dusty Saharan air in the layer between z_1 and z_2 , called the Saharan Air Layer (SAL).

4.1.1. The SAL Over the Ocean

[69] We can generalize to the tropical Atlantic Ocean the results of soundings over Sal and Guadeloupe (Figures 8 and 9), stating that between two successive tropical depressions, there is a low-level inversion of temperature (at level z_1). This inversion is related to the anticyclone that covers the north Atlantic during the event (Figure 1a). The subsidence of the anticyclonic air masses competes with the convection in the underlying marine layer [*Triplet and Roche*, 1971]. The altitude z_1 corresponds to the level of equilibrium, delimiting the convective and subsiding motions. This level rises from 1000 m at Sal to 1500–2000 m over the Caribbean Sea (Figures 8b, 8c, and 9a).

[70] Dust may be embedded between this low-level inversion and the inversion z_2 (Figures 8b, 8c, and 9a). Following *Carlson and Prospero* [1972], we call the Saharan Air Layer (SAL) this layer between z_1 and z_2 .

[71] The lack of convection above the altitude z_1 allows for the existence of a dry adiabatic transport layer between z_1 and z_2 over the ocean. Moreover, the mean values of the potential temperature θ in this transport layer are nearly identical, around 40°C , for Sal (Figure 9a) and Guadeloupe (Figures 8b and 8c). This reveals the adiabaticity of the SAL during its transport over the Atlantic.

4.1.2. A Dust Transport in the SAL

[72] From the reports of airplane pilots over Guadeloupe, we know that most of the dust was in a layer above 1500 m, corresponding to the SAL. The dependency between the photometric aerosol optical depth δ_A measured over Guadeloupe and the geometrical thickness ($z_2 - z_1$) of the SAL derived from the soundings, from 19 to 23 June, is roughly linear (Figure 15). In agreement with the results of *Carlson and Prospero* [1972], this linear dependency supports the argument that over Guadeloupe, the layer between z_1 and z_2 coincides with the dust layer. This is also a confirmation that the previously described back trajectory BT3200 was in the SAL, while BT1500 was outside it (in the depression ahead of the SAL at the beginning, then in the marine layer under the SAL at the end of the transport).

[73] However, dust is also observed in the marine layer, below z_1 . In particular, Figure 7 shows the decrease of the horizontal visibility, measured at the sea level, when the

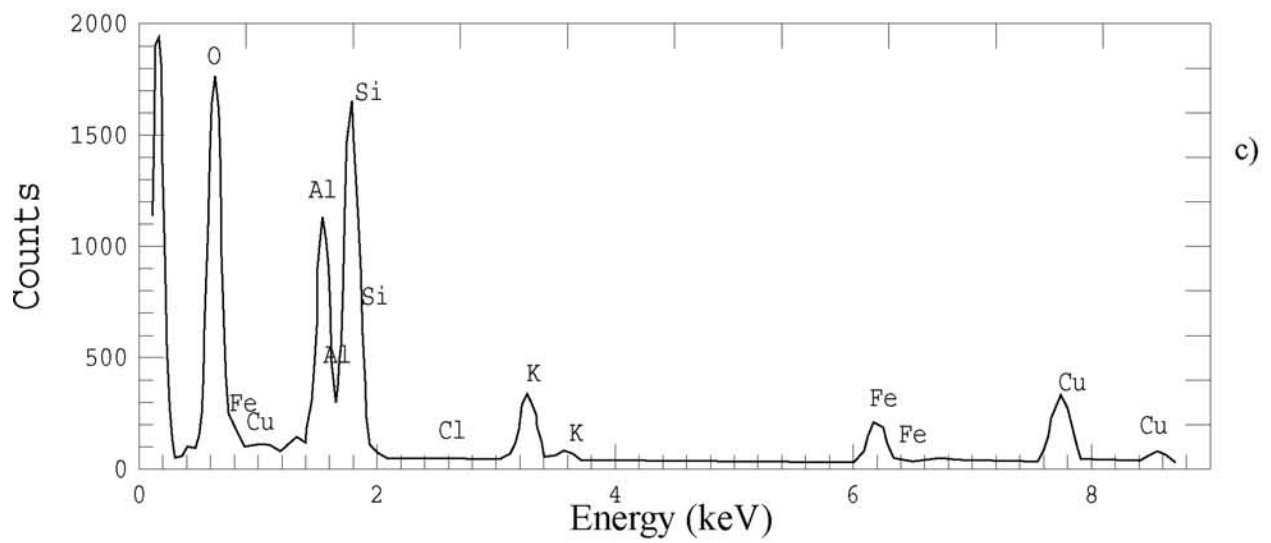
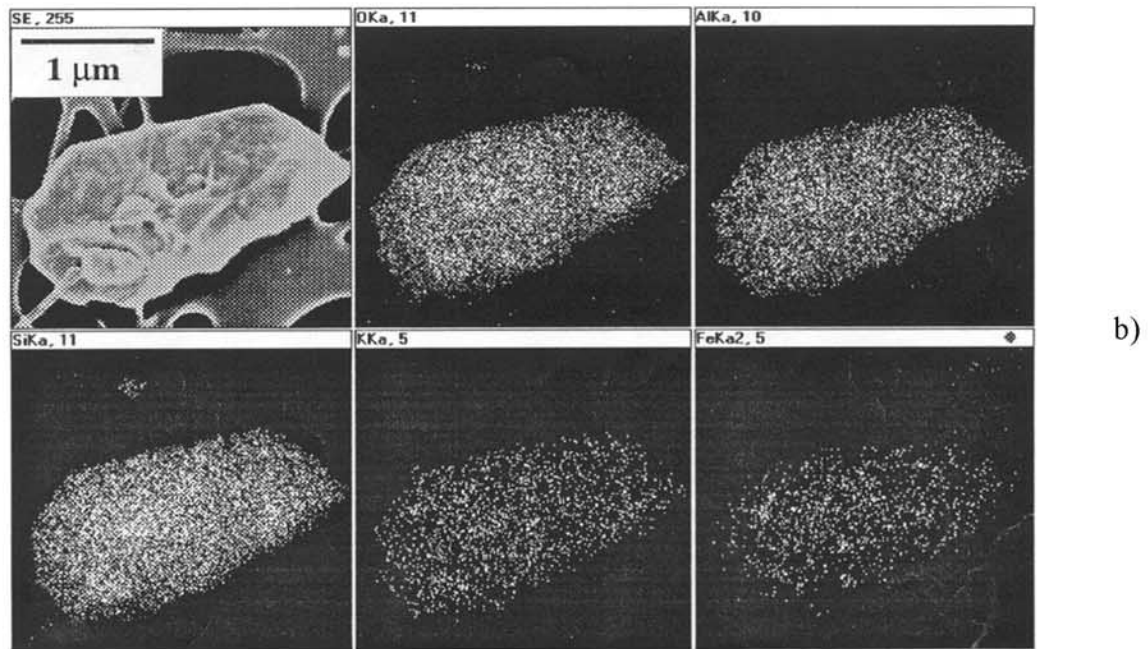
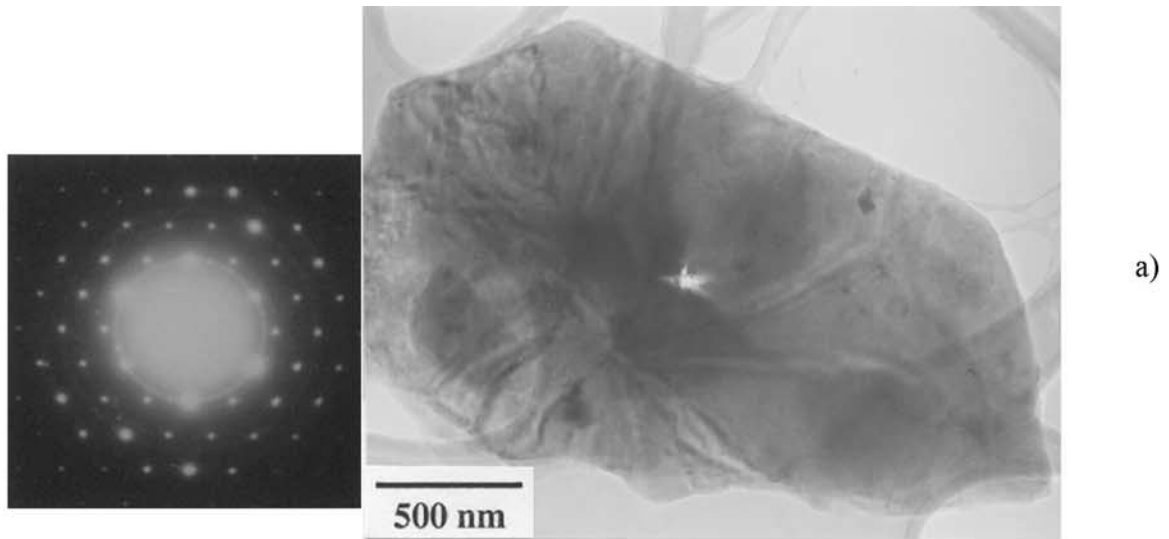


Figure 13

dust optical depth increases. This dust presence near the surface results from the sedimentation of particles by gravitation, from the overlying SAL, through the marine boundary layer. Figure 7 shows that the dust amount in the marine layer (related to the visibility reduction) increases with the optical depth, and hence (consistently) with the mass of dust transported in the overlying SAL.

4.1.3. Relation Between SAL and Dust

[74] Soundings over Guadeloupe showing a low-level temperature inversion (indicated with cyan stripes in Figure 5) are observed on 24 June, which does not appear obviously dusty as shown from satellite (Figure 4b) and photometric measurements (Figure 6). Expanding our investigation to the period from May to July 1994 during which photometric measurements were performed, we discovered that days with low-level temperature inversion could be associated to a large range of aerosol optical depth δ_A including low values (and high visibility values V) [MétéoFrance, 1994; R. Mazurie, personal communication, 1994]. In Table 2, we report the days of this period with $\delta_A < 0.2$ and $V \geq 25$ km, which can be considered dust free. Similar observations can be done at Sal.

[75] So, low-level T inversion days, associated with the presence of a SAL, are not systematically dusty (but conversely, we can check that dust presence is systematically associated with a low-level temperature inversion). The conclusion is that a SAL always exists between two easterly waves, whether dusty or not. Over Africa, dry hot air is lifted through convection from the arid desert surface to a high altitude. The lifted hot air masses can be dusty or dust-free according to the potential of the underlying soil to deflation and to the surface wind speed. Dusty or not, the Saharan air masses undergo subsidence above the level z_1 during their oceanic transport in the SAL (but they cannot be transported in a depression because of the deep convection at higher altitudes).

4.2. Dust Layer

[76] Dust transport can be studied from the air mass back trajectories starting from Guadeloupe. The dust source area deduced from these trajectories are in good agreement with those determined from satellite images. We also compare our results to the model of Saharan dust plume from Karyampudi *et al.* [1999].

4.2.1. Dust Uplift Above the Sources

[77] From the back trajectories, we see that the dusty air masses are lifted up to very high altitudes, around 5000 m, over Africa (Figure 11b). This agrees with a convective motion associated to a depression. The pressure maps from MétéoFrance show such a depression over Africa on 14 June (Figure 2a). The model from Karyampudi *et al.* [1999] predicts such an uplift in such conditions. From Bergametti [1987], the genesis of a dust plume over Saharan or sub-Saharan regions depends on the intensity of the surface wind and on the state of the underlying soil. In our study,

the following conditions appear to explain the strength of this dust event: (1) a relatively strong surface wind over 10 m s^{-1} (Figure 2b) associated with the presence of a depression (Figure 2a), over northern Mali and (2) a source region (determined from the IR satellite images (IDDI) and back trajectories) made up of erodible soil able to release large amounts of mineral particles.

4.2.2. Transport Over Ocean

[78] Figure 11a shows that over ocean, the back trajectories are directed toward east, and approximately parallel between 15 and 20°N , in agreement with the wind field at 850 hPa shown in Figure 1b for 18 June at 1200 UTC. We use them to deduce information about the transport from the dust source to Guadeloupe. As the trajectories pass over Sal where meteorological data are available, we can improve the description of the transport over the ocean.

[79] As in Figure 11b, the air masses regularly falls some $340 \pm 20 \text{ m d}^{-1}$ over the ocean for all the back trajectories arriving over Guadeloupe between 19 and 23 June, revealing a quasi-constant subsidence of the anticyclonic air masses. Such a result is remarkable, for a transport in a SAL characterized by a lower level (z_1) increasing in the direction of transport (Figures 8b, 8c, and 9a).

[80] The existence of such descending trajectories involves a condition for the presence of dust over Guadeloupe at a level higher than the low-altitude temperature inversion z_1 (1500–2000 m). Considering the transport time of 3.75 days between Sal and Guadeloupe, deduced both from back trajectories and satellite images, dust must leave Sal at an altitude higher than 3000 m (Figure 11b). If the dust plume is below this altitude over Sal, it cannot reach the Caribbean islands. As a conclusion, only high-altitude uplifts occurring over Africa in summer are responsible for long-range transport.

[81] These results are in agreement with the dust plume model proposed by Karyampudi *et al.* [1999], predicting also a westward sinking of the top of the dust layer associated with a westward rise of the bottom of this dust layer above a gradually deeper marine layer.

[82] We observe that the altitude of transport slightly decreases westward over the ocean (Figure 11b). Over Guadeloupe this layer is situated between 1500 and 4700 m, while it is between 1000 and 6000 m over Sal, 3 days before. In addition, the successive images of the dust plume over the ocean (Figure 4b) show a spreading of the plume. On the satellite images of 16 and 17 June (Figure 4b), the plume going west is observed to undergo an anticyclonic gyration, in agreement with the model described by Karyampudi *et al.* [1999].

4.3. Discussion of the Structure, Size Distribution, and Origin of the Particles

[83] Because of the short lifetime of the clouds (about 20 min), the capture of particles of the dust plume by cloud droplets (see section 3.7) might have occurred only near

Figure 13. (a) Transmission electron micrograph and electron diffraction pattern of a flat particle, showing its monocrystalline state. The white patch at the center of the picture corresponds to the size of the analytical probe used for the X-rays spectrum collection (Figure 13c). (b) Secondary electron image of the particle and corresponding elemental mappings (oxygen, aluminum, silicon, potassium, and iron). These analytical images show the homogeneous distribution of each element in the particle. (c) X-ray spectrum showing the presence of oxygen, aluminum, and silicon as major elements and potassium and iron as minor ones. The copper signal is due to the copper grid supporting the sample.

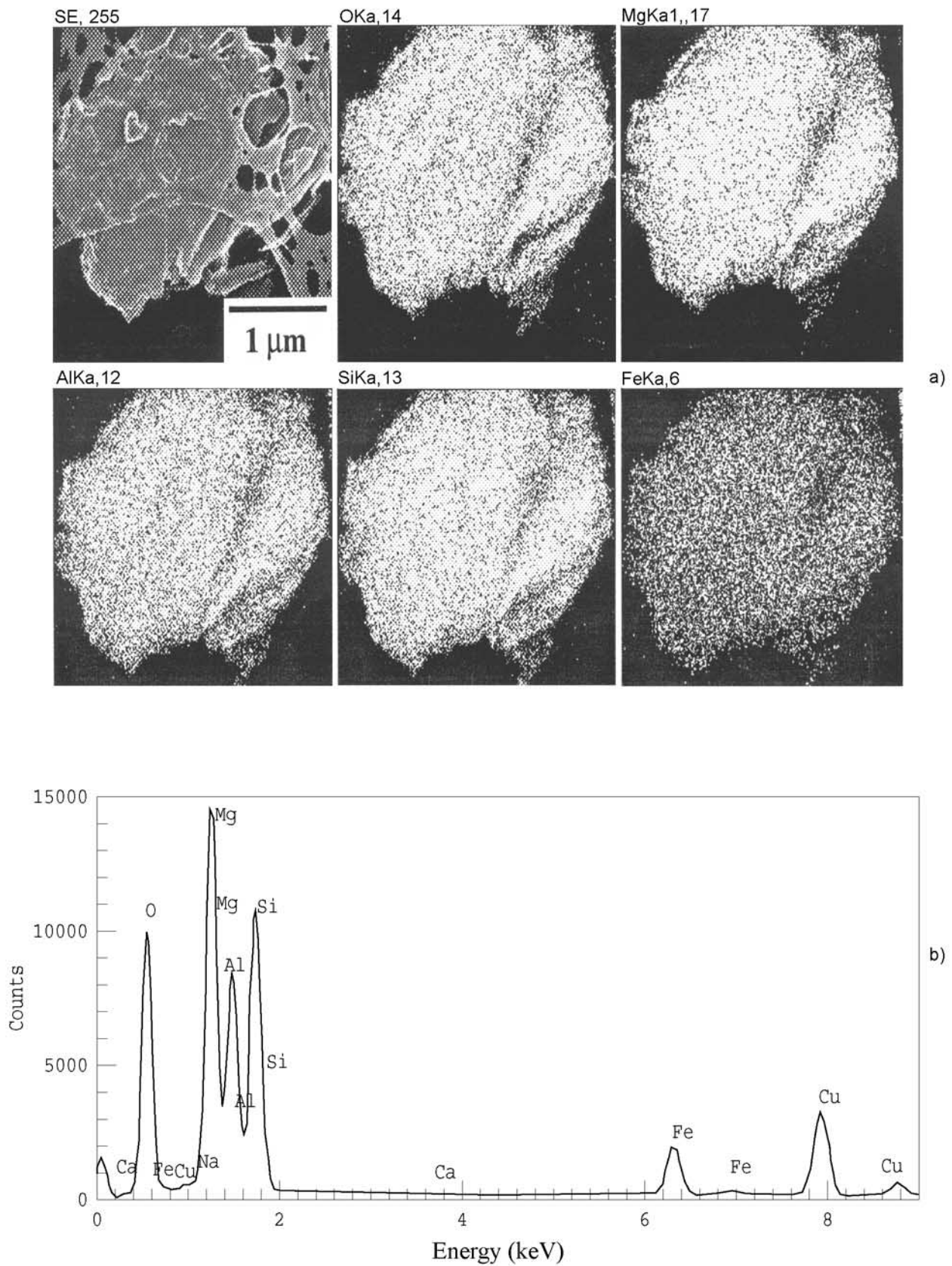


Figure 14. (a) Secondary electron micrograph, elemental mapping, and (b) X-ray spectrum recorded on a flat particle. The major (O, Al, Mg, Si) and minor (Fe) components are homogeneously distributed over the whole particle.

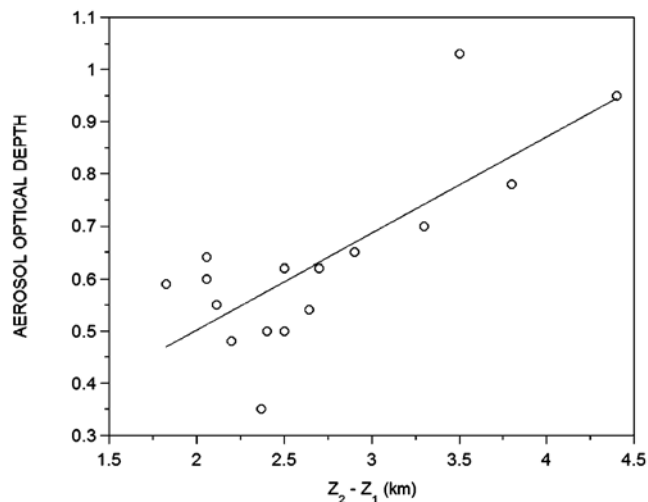


Figure 15. Aerosol optical depth δ_A for the dust event of 19 to 23 June 1994 (from Meteosat-3 VIS images over Guadeloupe at 1400 LST) versus difference (in km) between the altitudes z_2 and z_1 of the two temperature inversions (from the soundings at 0800 LST).

Guadeloupe. If we suppose that the particles collected in the rain samples have been transported up to the Guadeloupe in the SAL without noticeable modification of their physico-chemical and mineral characteristics, we can expect that after their short stay in water droplets (insofar they are not water soluble), they will have kept most of their initial properties.

[84] The direct (microscope) observation of relatively large particle, with a mean size close to $4 \mu\text{m}$ (Figure 12), proves that the Saharan mineral dust transported over the West Indies is not made up only with submicronic particles (it is even possible that submicronic particles constitute a marginal fraction of the distribution). This result is in agreement with the values close to zero of the Ångström exponent α_{1-2} revealing a presence of particles much larger than the photometric wavelengths. The size distribution shown in Figure 12 is consistent with the measurements of Prospero [1981b] in Barbados, a Lesser Antilles island, and with the results presented by Patterson and Gillette [1977]. It is also consistent with the retrievals from Aerosol Robotic Network (AERONET) measurements (website <http://aeronet.gsfc.nasa.gov/>) of the particle size distribution in the case of nonspherical particles [Dubovik et al., 2002a]. The elemental composition is comparable to that found by Prospero [1981b] and Glaccum and Prospero [1980] for particles reaching the Lesser Antilles islands and to those

Table 2. Days With a SAL and Without Dust (Low Aerosol Optical Depth, High Visibility) Between May and July 1994

Date 1994	δ_A at 870 nm	V, km
2 May	0.14	40
18 May	0.17	25–30
19 May	0.15	35
30 May	0.18	40
6 July	0.17–0.11	30

Table 3. Columnar Mass and Total Mass Over the Atlantic Ocean for 19 June 1994 Using the AERONET Particle Size Distribution Retrieved From the Measurements of the Guadeloupe Station for 20 June 2001 and Various Values of the Complex Index

Complex Index	$m/\delta_A, \text{g m}^{-2}$	M, Mt
$1.53 - 0.008i$	2.16	4.24
$1.53 - 0.003i$	2.18	4.27
$1.53 - 0.0006i$	2.19	4.29
$1.48 - 0.0006i$	2.28	4.47
$1.56 - 0.0006i$	2.13	4.19

of African origin measured over the Canary Islands [Coude-Gaussen et al., 1987].

4.4. Estimation of the Mass of Transported Dust

[85] For a given mineral composition of dust and for spherical particles characterized by a given size distribution, the aerosol optical depth varies linearly with the mass in the vertical column of atmosphere. In other words, the ratio of the columnar mass to the aerosol optical depth is a constant characterized by the particle size distribution and by the complex index of the mineral (or the mixture) of concern. So we can estimate the mass of dust over the north tropical Atlantic starting from the maps of satellite aerosol optical depth (Figure 4b) calculated at 640 nm for the background dust model of Shettle [1984]. With the usual values of 2500 kg m^{-3} for dust bulk density and assuming uniform size distribution and complex index all over the ocean, we calculate a column mass to aerosol optical depth ratio of 1.29 g m^{-2} . Summing up over the clear ocean area the column mass derived from the conversion of aerosol optical depth and assuming the aerosol optical depth has the same value on the average over clear and cloudy oceanic areas, we calculate for 19 June a total mass of 2.66 Mt over an ocean surface of about $3.6 \cdot 10^6 \text{ km}^2$.

[86] More recent radiometric measurements on mineral dust, especially those obtained from AERONET [Holben et al., 1998], show that the real part n of the complex index can be somewhat different of 1.53 and that its imaginary part k is significantly smaller than 0.008 (the values used for computing Figure 4b). Dubovik et al. [2002b], discuss AERONET retrieval results with n obtained in the range [1.48, 1.56] and k in the range [0.0006, 0.003]. In addition, the particle size distribution is also retrieved in the processing of AERONET measurements [Nakajima et al., 1983, 1996; Dubovik and King, 2000]. AERONET measurements took place in Guadeloupe in 1997 (Principal Investigator R.-H. Petit). We have selected the measurements of 20 June 2001 and calculated the column mass to aerosol optical depth ratio and the total mass over ocean, for various values of the complex index consistent with values of Dubovik et al. [2002b]. The results are shown in Table 3. The calculated mass are practically independent on k , and their variation with n is small. The range of the computed masses is [4.19, 4.47Mt], corresponding to a mass variation of $\pm 3\%$. However, the comparison of masses computed using AERONET retrievals with the computation using the dust model from Shettle, shows that the AERONET mass is larger by a factor 1.6. This large difference arises from a larger fraction of larger coarse particles in the size distribution from AERONET. So the uncertainty on the calculated

mass is not really due to the accuracy on the complex index, but it depends to a large extent on the accuracy of the determination of the particle size distribution.

[87] Using again the radiometric measurements from AERONET, it is possible to check the assumption of a uniform particle size distribution over the north tropical Atlantic with the data from the Cape Verde islands station (P.I.: D. Tanré). We have used the results from Table 1 of *Dubovik et al.* [2002b], for the Cape Verde islands. The particle size distributions for this station is not very different of the size distributions obtained for the Guadeloupe station. We calculate a total mass over the ocean of 4.7 Mt for the 19 June 1994, slightly more than with the data from the Guadeloupe station. So the change of the particle size distribution during dust transport through the Atlantic is limited and the previous assumption of a uniform particle size distribution over the north tropical Atlantic is realistic. We conclude that the total mass of this event is in the range 2.5–5 Mt.

[88] The previous mass values correspond to one of the four to five major dust events occurring each year. Combining such events with the numerous (up to 13, a mean value from 1993 to 2002) events of lower importance we can estimate a mean covered surface and aerosol optical depth for the major and minor events. This computation results in a total amount of dust transported each year over the Atlantic Ocean, comprised between 26 and 62 Mt yr⁻¹, taking into account the various uncertainties. The larger values correspond to the hypothesis of a same covered area for the plumes of all events. The smaller values correspond to areas proportional to the length of the outbreaks derived from the duration of the event over Guadeloupe.

5. Conclusion

[89] This study provides a comprehensive description of a dust plume transported across the Atlantic Ocean to Guadeloupe on 14–23 June 1994, since its genesis from a Saharan source until its final dispersion over the Caribbean Sea. For this, several complementary techniques have been applied and the consistency of the various results obtained can be estimated through their cross-checking.

[90] From IDDI images derived from Meteosat-5 IR data, a dust emission is located in SW Sahara and NW Sahel on 14 June at 1200 UTC. The back trajectories provided by MétéoFrance confirm a dust emission at the same time at the location (20.5°N, 2.5°W), close to the dry salty lake of Taoudenni, Mali. This region is characterized by a threshold of wind velocity for dust emission of 7–8 m s⁻¹ [*Martcorena et al.*, 1997], lower than the surface wind speed of 10 m s⁻¹ reported by MétéoFrance maps. It belongs to a major dust source, active in summer [*Brooks and Legrand*, 2000].

[91] Photometric measurements performed in Guadeloupe indicate high values of dust optical depth during the period 19–22 June, with a maximum close to 1 on 21 June. These results are in close agreement with the values derived from Meteosat-3 VIS in the vicinity of the island.

[92] Dust over Guadeloupe contains a significant fraction of large particles, as indicated by values close to zero of the Ångström exponent derived from the photometric measurements, and confirmed by direct microscope observation

which provides a modal particle size of 4 μm (no reliable result on the presence and size of fine particles can be given). The structure and composition deduced from electron diffraction and microscopy are those of African dust.

[93] Using the photometer and Meteosat-3 VIS data, along with complex indices and particle size distributions either for the background mineral dust model of *Shettle* [1984] or derived from AERONET measurements, provides estimates of the mass of dust transported over the Atlantic Ocean in the range [2.5–5 Mt].

[94] The back trajectories indicate that the source emission is followed by a steep ascending motion of the hot dusty air masses up to 5000 m over Africa. After their expulsion over the Atlantic, the dusty air masses (constituting then the SAL) undergo a slow smooth descending motion from 5000 to 3200 m during their westward travel to the Caribbean Sea. This subsidence is confirmed by the meteorological soundings performed at Sal and Guadeloupe, indicating in addition a thinner SAL thickness over Guadeloupe than over Sal. It is inferred from this subsiding motion that only high-altitude uplifts of dusty air masses (at least at 3000 m over the Cape Verde islands) can result in a long-range transport (up to Guadeloupe). The back trajectories as well as the dust optical depth maps derived from Meteosat-3 VIS show that transport from Sal to Guadeloupe lasted 3.75 days (and 4.25 days from the African coast).

[95] Comparison of geometrical thickness of the SAL with photometric dust optical depth suggests that dust was mostly located within the SAL (confirmed by pilots' observations). However, the underlying marine layer was simultaneously loaded with dust particles (revealed by visibility measurements), as was the water from rainfall following the dust event (measured from analyzed rain samples). This results from the dry settling of the larger particles through gravity, and from the scavenging by cloud droplets and washout by rain drops.

[96] Extending the period of study over the rainy season in Guadeloupe and Sal shows that the presence of a SAL (revealed by the static energy from the soundings) is not always associated with the presence of dust. To be dusty, the Saharan air masses must be lifted from the source areas in the presence of a sufficiently strong surface wind speed, then relayed through convection.

[97] **Acknowledgments.** The authors are grateful to Roland Mazurie from MétéoFrance, Center of Guadeloupe, for his fruitful discussions and kind assistance. They also thank the director of the Serviço Nacional de Meteorologia i Geofísica (SNMG) at Sal island. The back trajectories have been calculated by Alain Pinault, from the Service Central d'Exploitation de la Météorologie, Toulouse, France. We want to thank him for his help. We thank Philippe Frayssinet and Emilie Miot from MétéoFrance, Toulouse, who provided us graciously with archive maps of winds and pressure. The satellite images have been processed using Mgraph and Msphinx designed by Louis Gonzales and Christine Deroo (LOA). Thanks are due to Nick Brooks, who helped us to improve significantly the manuscript by refining the English. We thank the NOAA and its service responsible of the HYSPLIT model (<http://www.arl.noaa.gov/ready/hysplit4.html>) for the free and easy supply of back trajectories they offer.

References

- Aspliden, C. (1972), Analyses de structures énergétiques lors de BOMEX, report, Barbados Oceanogr. and Meteorol. Exp., NOAA, Tallahassee, Fla.
- Bergametti, G. (1987), Apports de matières par voie atmosphérique à la Méditerranée occidentale: Aspects géochimiques et météorologiques, thèse de doctorat, Univ. Paris 7, Paris.

- Brooks, N., and M. Legrand (2000), Dust variability over northern Africa and rainfall in the Sahel, in *Linking Climate Change to Landsurface Change*, edited by S. J. McLaren and D. Kniveton, pp. 1–25, Springer, New York.
- Carlson, T. N., and J. M. Prospero (1972), The large scale movement of Saharan air outbreaks over the northern equatorial Atlantic, *J. Appl. Meteorol.*, *16*, 1368–1371.
- Coakley, J. A., Jr., and F. P. Bretherton (1982), Cloud cover from high-resolution scanner data: detecting and allowing for partially filled fields of view, *J. Geophys. Res.*, *87*, 4917–4932.
- Coude-Gaussen, G., P. Rognon, G. Bergametti, L. Gomes, B. Strauss, J. M. Gros, and M. N. Le Coustumer (1987), Saharan dust on Fuerteventura islands (Canaries): Chemical and mineralogy, air masses trajectories and probable sources, *J. Geophys. Res.*, *92*, 9753–9771.
- D'Honneur, G. (1979), *Traité de Météorologie Tropicale*, Dir. de la Météorol., Trappes, France.
- Dubovik, O., and M. D. King (2000), A flexible inversion algorithm for retrieval of aerosol optical properties from Sun and sky radiance measurements, *J. Geophys. Res.*, *105*, 20,673–20,696.
- Dubovik, O., B. N. Holben, T. Lapyonok, A. Sinyuk, M. I. Mishchenko, P. Yang, and I. Slutsker (2002a), Non-spherical aerosol retrieval method employing light scattering by spheroids, *Geophys. Res. Lett.*, *29*(10), 1415, doi:10.1029/2001GL014506.
- Dubovik, O., B. N. Holben, T. F. Eck, A. Smirnov, Y. J. Kaufman, M. D. King, D. Tanre, and I. Slutsker (2002b), Variability of absorption and optical properties of key aerosol types observed in worldwide locations, *J. Atmos. Sci.*, *59*, 590–608.
- Glaccum, R. A., and J. M. Prospero (1980), Saharan aerosols over the tropical North Atlantic mineralogy, *Mar. Geol.*, *37*, 295–321.
- Holben, B. N., et al. (1998), AERONET: A federated instrument network and data archive for aerosol characterization, *Remote Sens. Environ.*, *66*, 1–16.
- Jankowiak, I., and D. Tanré (1992), Satellite climatology of Saharan dust outbreaks: Method and preliminary results, *J. Clim.*, *5*, 646–656.
- Karyampudi, V. M., et al. (1999), Validation of the Saharan dust plume conceptual model using lidar, Meteosat and ECMWF data, *Bull. Am. Meteorol. Soc.*, *80*, 1045–1075.
- Legrand, M., G. Cautenet, and J. C. Buriez (1992), Thermal impact of Saharan dust over land. part II: Application to satellite IR remote sensing, *J. Appl. Meteorol.*, *31*, 181–193.
- Legrand, M., C. N'doumé, and A. Plana-Fattori (2001), Satellite detection of dust using the IR imagery of Meteosat: 1. Infrared difference dust index, *J. Geophys. Res.*, *106*, 18,251–18,274.
- Marticorena, B., G. Bergametti, B. Aumont, Y. Callot, C. N'doumé, and M. Legrand (1997), Modelling the atmospheric dust cycle: A simulation of Saharan dust sources, *J. Geophys. Res.*, *102*, 4387–4404.
- MétéoFrance (1994), *Tableau Climatologique Mensuel, mai à Septembre 1994*; Aéroport du Raizet, Pointe à Pitre, Guadeloupe.
- Molinié, J. (1991), Les ondes d'Est, *Colloque "Les ouragans de l'Atlantique"*, Pointe à Pitre, Guadeloupe.
- Nakajima, T., M. Tanaka, and T. Yamauchi (1983), Retrieval of the optical properties of aerosols from aureole and extinction data, *Appl. Opt.*, *22*, 2951–2959.
- Nakajima, T., G. Tonna, R. Rao, P. Boi, Y. Kaufman, and B. Holben (1996), Use of sky brightness measurements from ground for remote sensing of particulate dispersion, *Appl. Opt.*, *35*, 2672–2686.
- Patterson, E. M., and D. A. Gillette (1977), Commonalties in measured size distribution for aerosols having a soil derived component, *J. Geophys. Res.*, *82*, 2074–2082.
- Petit, R.-H., J. Molinié, S. Jacoby-Koaly, and D. Bernard (2001), Ground temperature and dust plume over Guadeloupe, paper presented at IAMAS 2001 Assembly, Session: Radiative Transfer, Validating Remote Sensing, Results, Innsbruck, Austria, 10–18 July.
- Prospero, J. M. (1981a), Eolian transport to the world ocean, in *The Sea*, vol. 7, *The Oceanic Lithosphere*, edited by C. Emiliani, pp. 801–874, Wiley Interscience, New York.
- Prospero, J. M. (1981b), Arid regions as sources of mineral aerosols in the marine atmosphere, *Bull. Geol. Soc. Am.*, *186*, 71–86.
- Prospero, J. M., and T. N. Carlson (1972), Vertical and areal distribution of Saharan dust over the western equatorial North Atlantic Ocean, *J. Geophys. Res.*, *77*, 5255–5265.
- Prospero, J. M., R. A. Glaccum, and R. T. Nees (1981), Atmospheric transport of soil dust from Africa to South America, *Nature*, *289*, 570–572.
- Shettle, E. P. (1984), Optical and radiative properties of a desert aerosol model, in *Proceedings of Symposium on Radiation in the Atmosphere*, edited by G. Fiocco, pp. 74–77, A. Deepak, Hampton, Va.
- Triplet, J. P., and G. Roche (1971), *Météorologie Générale*, Ecole Natl. de la Météorol., Toulouse, France.

C. Asselin de Beauville, G. Marion, J. Molinié, and R. H. Petit, Laboratoire de Physique de l'Atmosphère Tropicale, Université Antilles Guyane, Pointe à Pitre, Guadeloupe 97159, French West Indies. (rosahelen.petit@univ-ag.fr)

I. Jankowiak and M. Legrand, Laboratoire d'Optique Atmosphérique, Université des Sciences et Technologies de Lille, F-59655 Villeneuve d'Ascq, France. (michel.legrand@univ-lille1.fr)

J. L. Mansot, Groupe de Technologie des Surfaces et Interfaces EA 24-32, Université Antilles Guyane, Pointe à Pitre 97159, Guadeloupe, French West Indies.